Interaction between Human Telomere and a Carbazole Derivative: A Molecular Dynamics Simulation of a Quadruplex Stabilizer and Telomerase Inhibitor[†]

Dah-Yen Yang[§], Ta-Chau Chang[§], and Sheh-Yi Sheu*,[‡]

Department of Life Sciences and Institute of Genome Sciences, Institute of Bioinformatics, and Structural Biology Program, National Yang-Ming University, Taipei 112, Taiwan, and Institute of Atomic and Molecular Science, Academia Sinica, Taipei 106, Taiwan

Received: March 11, 2007

The mechanism of inhibition of telomerase by drugs is a key factor in an understanding of guanine-quadruplex complex stabilization during human cancer. This study describes a simulated annealing docking and molecular dynamics simulation to investigate a synthesized potent inhibitor, 3,6-bis(1-methyl-4-vinylpyridinium iodine) carbazole (BMVC), which stabilizes the quadruplex structure of the human telomeric DNA sequence d[AG$_3$(T$_2$AG$_3$)$_3$] and inhibits telomerase activity. The compound was predicted to selectively interact with the quadruplex structure. During our simulation, the binding affinities were calculated and used to predict the best drug-binding sites as well as enhanced selectivity compared with other compounds. Our studies suggest that the simulation results quite coincide with the experimental results. In addition, molecular modeling shows that a 2:1 binding model involving the external binding of BMVC to both ends of the G-quartet of d[AG$_3$(T$_2$AG$_3$)$_3$] is the most stable binding mode and this agrees with the absorbance titration results that show two binding sites. Of particular interest is that one pyridinium ring and carbazole moiety of the BMVC can stack well at the end of G-quartet. This implies that BMVC is a good human quadruplex stabilizer and also a good telomerase inhibitor.

I. Introduction

At the two ends of the chromosomes of eukaryotes, the noncoding regions of DNA are called telomeres.[1] It is well-known that telomeric function plays a key role during cell replication processes such as recombination and degradation.[2] In normal cells, typically, telomeres shorten in length in somatic cells with each round of replication, and this is as a consequence of the inability of DNA polymerase to fully replicate the ends. Usually, 50–200 bases are lost at each round of cell division. Once telomeres reach a critically short length, cells enter a senescent state and do not replicate further.[3] In contrast, in tumor cells, the length of telomeres is highly conserved and maintained by the action of a DNA polymerase.[4] People now realized that telomerase, a protein of about 170 kDa, catalyzes the elongation of the telomere repeats. Therefore, telomerase is activated in 80% to 90% of tumor cells and is undetectable in most normal somatic cells.[2,5] In previous studies,[6,7] the authors have shown that the inhibition of telomerase overcomes the ability of cells to proliferate and leads to cell death in tumors. This suggests that telomerase is a potent anticancer drug target.[8,9]

As far as we know, the telomeric DNA consists of simple tandem repeats of guanine (G)-rich sequences, which are typified by the hexanucleotide d(TTAGGG)n in vertebrates.[10,11] This G-rich telomeric repeat is known to have been conserved over evolutionary time. In eukaryotes, the telomere length of the repeat TTAGGG is between about 5 kb and 15 kb.[1,2] In this region of telomeric DNA, the tandem repeats of the G-rich sequences fold into a quadruplex structure. All quadruplexes contain a basic repeating and stacking motif, the G-quartet structure, which is formed by four guanine bases and held in a plane by Hoogsteen hydrogen bonds.[12]

One possible direct end product of this is the functioning of the guanine-rich telomeric DNA in a process by which the chromosome ends are protected from unwanted DNA damage, DNA repair, recombination, and end-fusions.[1,13,14] Furthermore, the folded telomeric DNA quadruplex structures have been shown to inhibit the enzyme that catalyzes the elongation of telomere repeats. Therefore, a designed compound that can stabilize such G-quartet structures may be a good candidate for an effective telomerase inhibitor and a potential therapeutic agent in many human cancer diseases.[9,13] There are quite a number of synthesized compounds that possess a planar aromatic chromophore, and these have been used to study the stabilization and binding affinity of folded quadruplex structures.[15] Based on extended amido-anthraquinone derivatives[16] and diben-zophenanthroline derivatives,[17] our studies suggest that the biological activity can be related to *in vitro* measurements using a modified TRAP assay, binding affinity, and increases in melting temperature.

In the present work, we performed a molecular dynamics simulation to calculate relative binding energies and these were used to predict the most effective drug-binding sites and any enhanced selectivity for a number of compounds.[16,17] A novel synthesized molecule, 3,6-bis(1-methyl-4-vinylpyridinium) carbazole diiodide (BMVC),[18] was used to interact with the human 22-mer telomeric DNA single strand d[AG$_3$(T$_2$AG$_3$)$_3$] (Hum22), and the results showed that this molecule could thermally stabilize the G-quadruplex structure. A range of experimental observations have found a significant increase in fluorescence and distinctive changes in fluorescence properties when BMVC

[†] Part of the "Sheng Hsien Lin Festschrift".
* Corresponding author. Tel: 886-2-28267233. Fax: 886-2-28234898. E-mail: sysheu@ym.edu.tw.
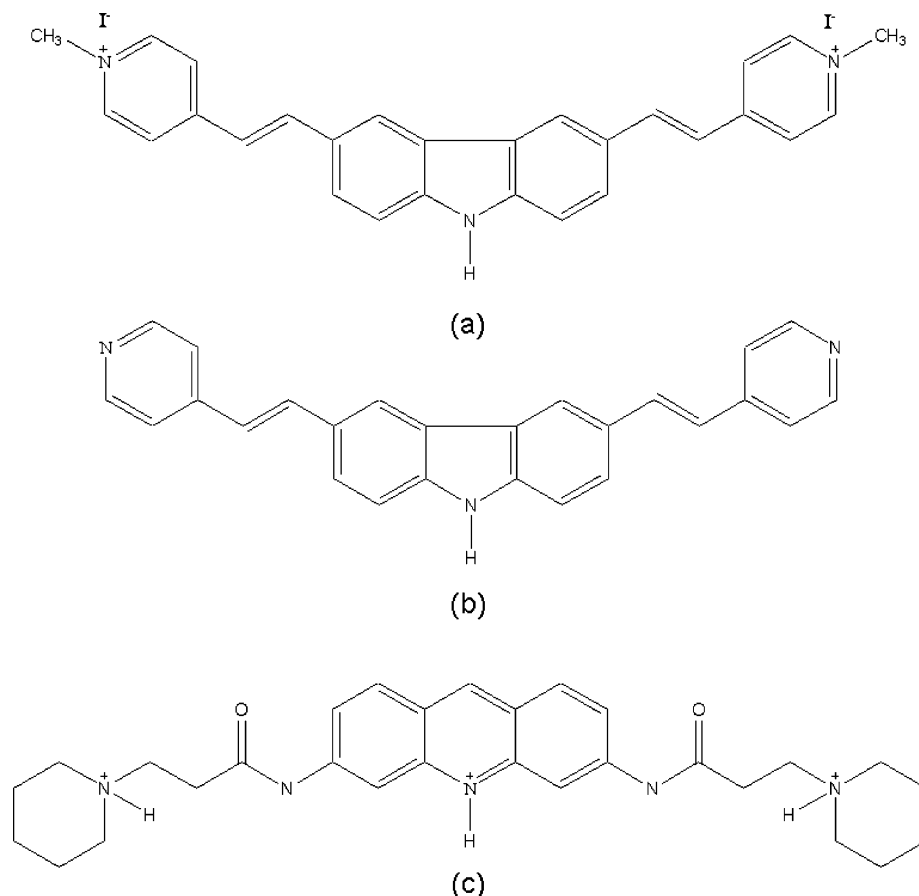[‡] National Yang-Ming University.
[§] Academia Sinica.

Human Telomere and Carbazole Derivative Interaction

J. Phys. Chem. A, Vol. 111, No. 38, 2007 **9225**

Figure 1. (a) The structure of BMVC. (b) The structure of the precursor of BMVC (PBMVC). (c) The structure of the acridine chromophore (AC).

TABLE 1: The Binding Energies (kcal/mol) for BMVC[a]

position (subset definition)	BMVC + DNA		BMVC + DNA binding energy
	vdW	electrostatic	
parallel loop (G4,T5,T6,A7,G8,G16,T17,T18,A19,G20)	−114.40	−13.77	−128.17
diagonal loop (A1,G2,G10,T11,T12,A13,G14,G22)	−104.25	−13.12	−117.37
wide groove (A1,G2,G3,G4,T5,T6,A7,G8,G9,G10,T11,T12)	−70.16	−13.24	−83.40
L shape on wide groove (G2,G3,G4,T5,T6,A7,G8,G9,G10)	−67.42	−12.94	−80.36
narrow groove (A13,G14,G15,G16,T17,T18,A19,G20,G21,G22)	−62.18	−13.09	−75.27
top parallel loop (T5,T6,A7,T17,T18,A19)	−44.88	−12.62	−57.50
parallel loop + diagonal loop (A1,G2,G4,T5,T6,A7,G8,G10,T11,T12,A13,G14,G16,T17,T18,A19,G20, G22)	−221.24	−23.58	−244.82

[a] Here we use the implicit water system with a dielectric constant of 78 after a simulated annealing docking process.

binds to DNA structures.[19−21] Experimental results[18] show that the melting temperature of the G quadruplex is remarkably increased by 13 °C on interaction with BMVC and there is a high binding affinity of the order of 10^9 M^{-1} *in vitro*.[22] In addition, an experimental assay by Lin and his co-workers[23] suggests that BMVC has a low telomerase IC$_{50}$ value (concentration required to inhibit cell growth by 50%) of about 0.1 μM compared with the other compounds.[15a,16e,17,24−27] Analysis also shows that absorbance titration typically indicates the presence of at least two binding sites for BMVC when it interacts with the G quadruplex d(T$_2$AG$_3$)$_4$.[18] Thus, it appears that BMVC interacts and thermally stabilizes the folded G-quadruplex structure. The aim of this work is to identify the mechanism of

interaction of the drug and the telomere sequence and to use this to help the design of new, more potent and improved stabilizers of the telomere structure. Such structure-based drug design has recently had important impacts on the development of antitumor drugs.

The outline of this paper is as follows. In section II, the molecular modeling and molecular dynamics simulation methods are introduced. In section III, the results of the molecular dynamics simulation are summarized and the various possible binding sites for BMVC are discussed. Our simulation results strongly support the experimental results that have been obtained previously, and a brief conclusion drawing on this is presented in section IV.
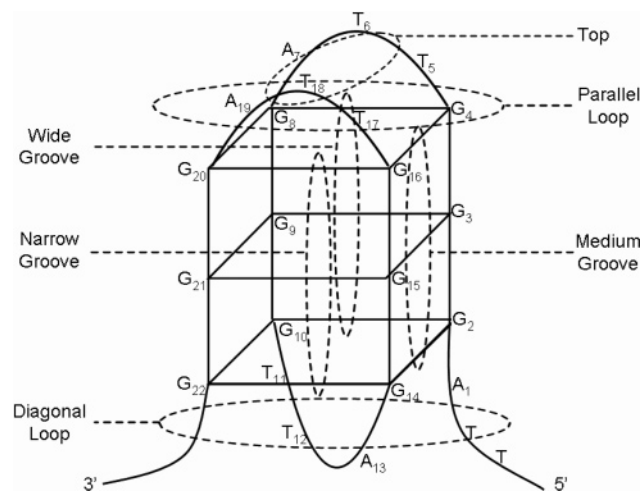
Figure 2. Sketch of the G-quadruplex structure of human 22 telomeric DNA. The BMVC binding sites are shown as circles and are indicated.

II. Computational Methods

In this work, all of the molecular modeling and dynamics simulations for the complexes of the quadruplex of the human 22-mer telomeric DNA single strand d[AG$_3$(T$_2$AG$_3$)$_3$] (Hum22) and BMVC for both external and internal intercalation sites were performed using the software InsightII[28a] and the CVFF force field.[28b] At the start, the initial structure of the Hum22 telomeric d[AG$_3$(T$_2$AG$_3$)$_3$] was taken from one of the solution NMR structures for folded intramolecular G-quadruplex structures stored at Protein Data Bank code 143D.[29] The sodium ions were inserted into the quartet planes and then the restraint tether force was set at 150 kcal/mol·Å for the system. Our system was subjected to energy minimization with 2000 steps of steepest descent (SD), and this was followed by 2000 steps of conjugate gradient (CONJ). The minimized structure thus produced was used as the initial structure for all studies herein. At the same time, an optimized geometry for BMVC was built up and the charge was calculated using the semiempirical MOPAC module in Insight II.

A fixed approach to docking and simulated annealing (SA) was adopted to identify the binding sites and study the binding interactions of the compounds with the G-quadruplex structure. We also introduced an intercalation ligand binding site between the diagonal T$_2$A loop and the G-quartet segment of the structure. Next, the minimized BMVC was manually docked into the binding sites. The positions and orientations of the BMVC in the binding sites were optimized using the AFFINITY module to ensure a starting model with low energy. This method incorporates manual and automatic docking procedures and allows nonbonded van der Waals and electrostatic interactions to be monitored during the docking so that as many conformations as possible could be interactively evaluated. Furthermore, flexible ligand docking also was used to define the lowest energy position for the BMVC using a Monte Carlo automated docking protocol. During these processes, the G quartets were restrained to their original positions throughout the docking protocols. During the simulation procedure, the BMVC atoms and receptor binding site atoms were movable. As a result, a number of possible conformations were evaluated. A similar search procedure was also made for other high-affinity ligand binding sites on the quadruplex. Finally, we found the final lowest energy conformation of the G-quadruplex−drug complex and this was then subjected to a further 200 steps of SD with unrestrained molecular energy minimization. The end product of the above process was used as an initial model for further studies.
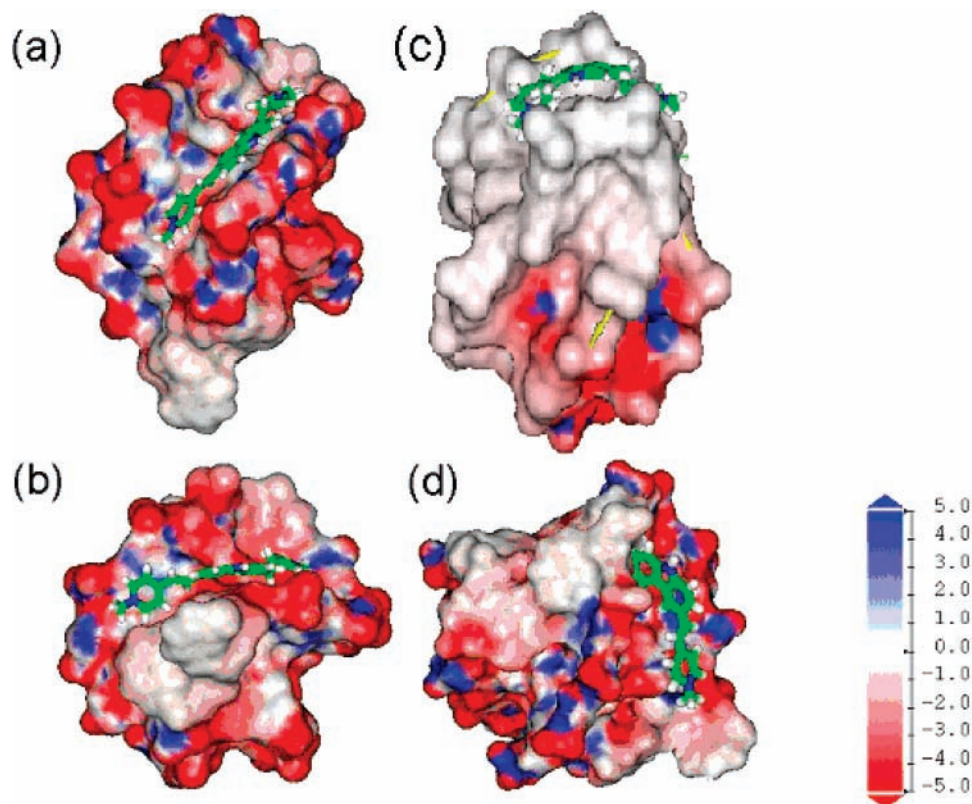

Figure 3. Plots of the minimized complex structures and surface electrostatic potential at the various possible binding sites: (a) narrow groove, (b) wide groove, (c) top parallel loop, and (d) L shape wide groove.
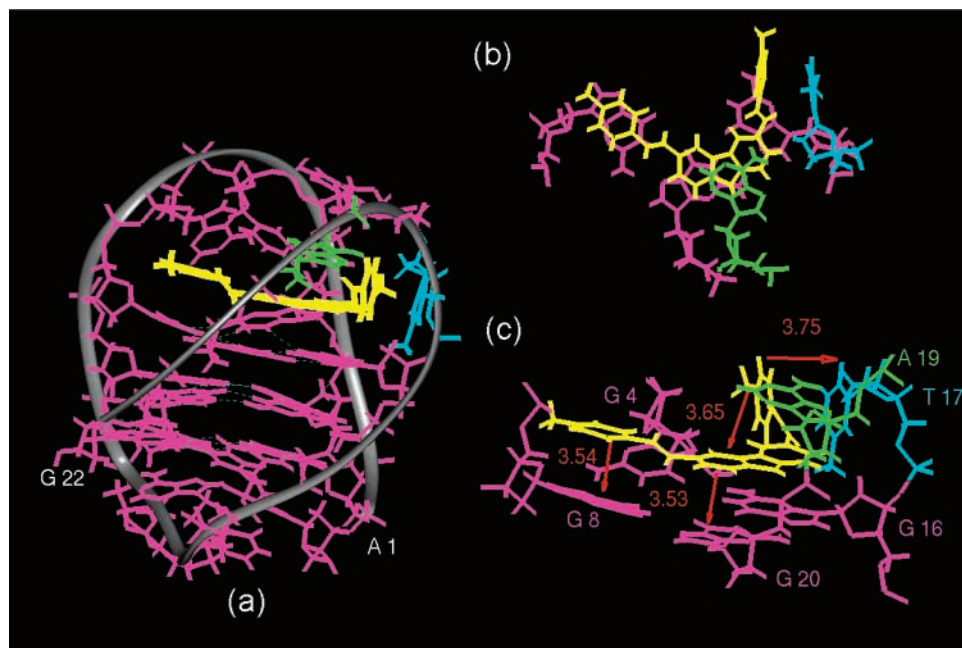
Human Telomere and Carbazole Derivative Interaction

J. Phys. Chem. A, Vol. 111, No. 38, 2007 **9227**

Figure 4. (a) A plot of the structure of BMVC and the G-quadruplex complex in the parallel loop from the molecular dynamics simulation. (b and c) Two different views of the binding site extracted from plot a.
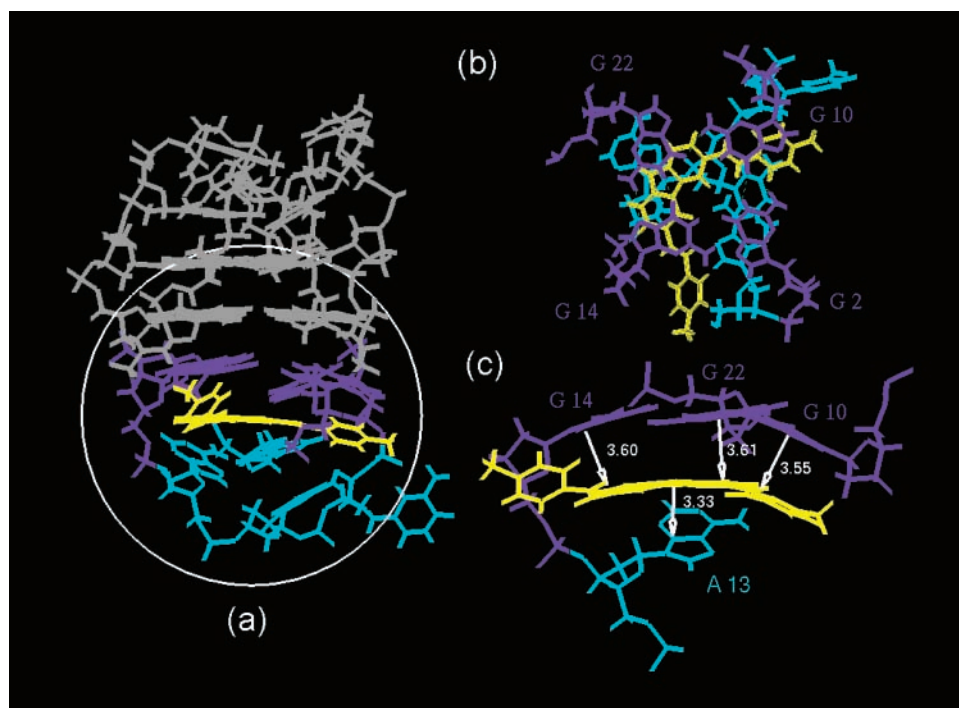

Figure 5. (a) A plot of the structure of BMVC and the G-quadruplex complex in the diagonal loop from the molecular dynamics simulation. (b and c) Two different views of the binding site extracted from plot a.

TABLE 2: The Stacked Distances (Å) for BMVC in the End-Stacked G Quartets[a]

position in parallel loop	stacked distance (Å)	position in diagonal loop	stacked distance (Å)
BMVC (carbazole)···G20	3.53	BMVC (carbazole)···G22	3.61
BMVC (pyridinium)···G8	3.54	BMVC (carbazole)···G14	3.60
BMVC (pyridinium)···T17	3.75	BMVC (pyridinium)···G10	3.55
BMVC (carbazole)···A19	3.65	BMVC (carbazole)···A13	3.33

[a] The stacked distance was identified after the molecular dynamics simulation.

Subsequently, the minimized G-quadruplex−drug complex was embedded in a TIP3P[30] water box of dimensions with 40.0 × 40.0 × 40.0(Å³) with 1717 water molecules. For this part of the study, we adopted a periodic boundary condition and 20 extra sodium ions and four chlorine counterions were added to neutralize the system. The temperature was set to 300 K and the cell multipole method[31] was used to treat the long-range electrostatic interactions during our calculations. In all of the
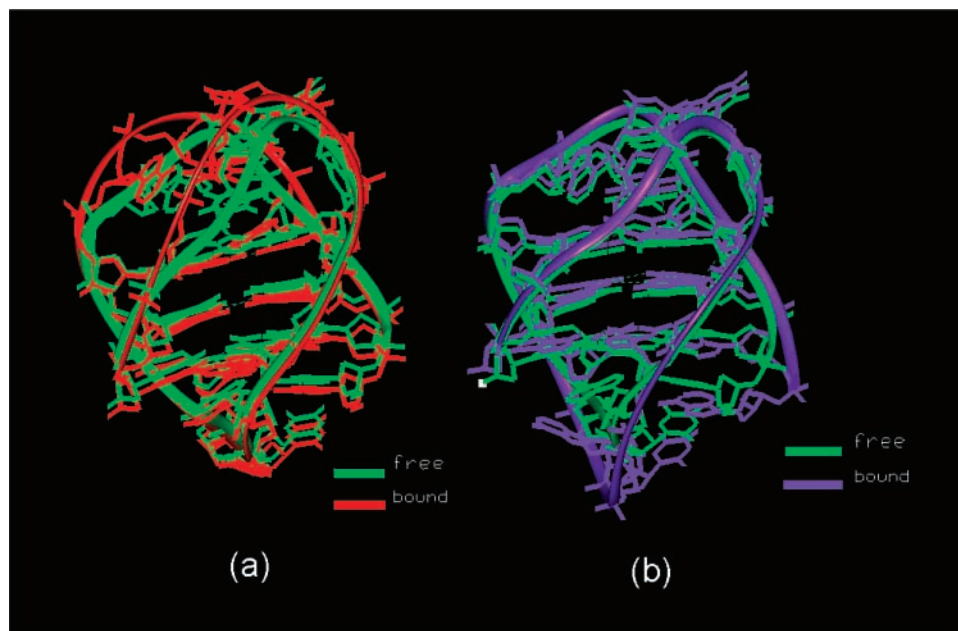
Figure 6. A comparison of the conformation of BMVC bound and free structures of the G-quadruplex structures (a) in the parallel loop and (b) in the diagonal loop. The green ribbon shows the free G-quadruplex structure. The red ribbon shows the bound G-quadruplex structure with BMVC in the parallel loop. The purple ribbon shows the bound G-quadruplex structure with BMVC in the diagonal loop.
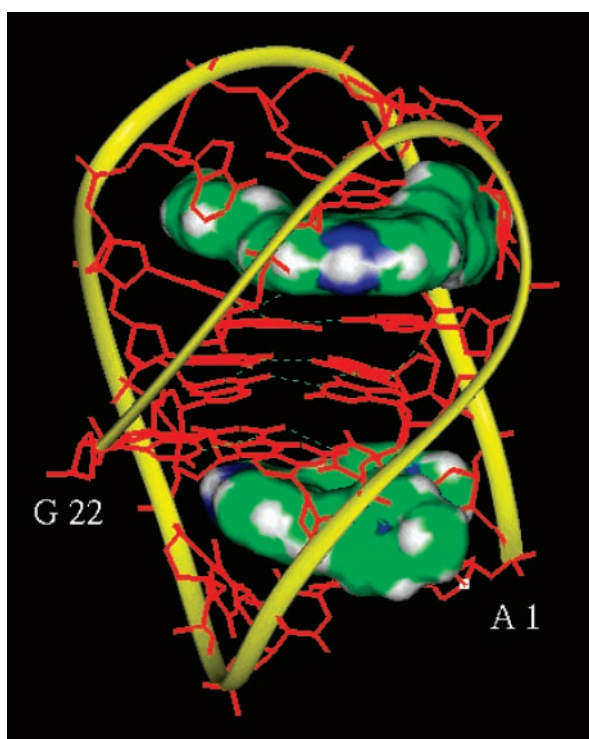

Figure 7. Plot of the structure of the 2:1 model where the two BMVCs are bound with one G quadruplex in the end-stacked model.

molecular dynamics simulations, in order to constrain the bond lengths involving the hydrogen atoms, the SHAKE algorithm[32] was applied. In each simulation, the time step was set to 1 fs in order to integrate out of the equations any motion by the molecules. For dynamic runs after minimizations, the initial velocities were assigned using the standard Maxwellian distributions.

Each complex system was separately subjected to 2000 steps of SD and CONJ energy minimization, followed by 2 ps of molecular dynamics to heat up the system temperature from 0 to 300 K. This was followed by a further 20 ps of equilibrium

dynamics with the restraint tether force set at 150 kcal/mol·Å for the complex system except for water molecules. In total, 30 ps of simulation dynamics was performed to gradually remove restraint. A further 20 ps production simulation run was used to analyze the ligand binding affinity.

For the drug only system, the starting model was taken from the minimized combined G-quadruplex−drug complex from which the G quadruplex had been removed. The computational protocol was the same as described in the preceding paragraphs for the complex system without restraint.

We also evaluated the nonbonding interaction energy between the G quadruplex and the drug by a direct calculation using the DOCKING module. During our computation, the relative binding affinity for all the models was calculated essentially by subtracting the total averaged interaction energy of the explicitly solvated drug and its surroundings in a neutral periodic box with identical systems, while the ligand was bound to the folded human G-quadruplex structure.

III. Results and Discussion

In this work, to unravel whether quadruplex stabilization plays a key role in the interaction between stabilizer and G quadruplex, we have focused on studying a synthesized compound BMVC (see Figure 1a) and its interaction with the G-quadruplex structure of human telomeric DNA sequence of d[AG$_3$(T$_2$AG$_3$)$_3$] using molecular modeling and a molecular dynamics simulation method. First of all, in order to screen for the best binding sites, we directly performed SA docking to calculate the nonbond interaction between BMVC and the DNA in the implicit water system. Our calculated binding energies are listed in Table 1. According to these, it was possible to predict by calculation where the best drug-binding sites are positioned and how to enhance selectivity of this molecule compared to other compounds.

Based on higher ranking after the SA docking process, several apparent binding sites of BMVC bound to the G-quadruplex of Hum22 telomeric DNA were identified and are shown in Figure 2. There are seven major binding sites made up of two end-stacked quadruplex (parallel loop and diagonal loop), one wide
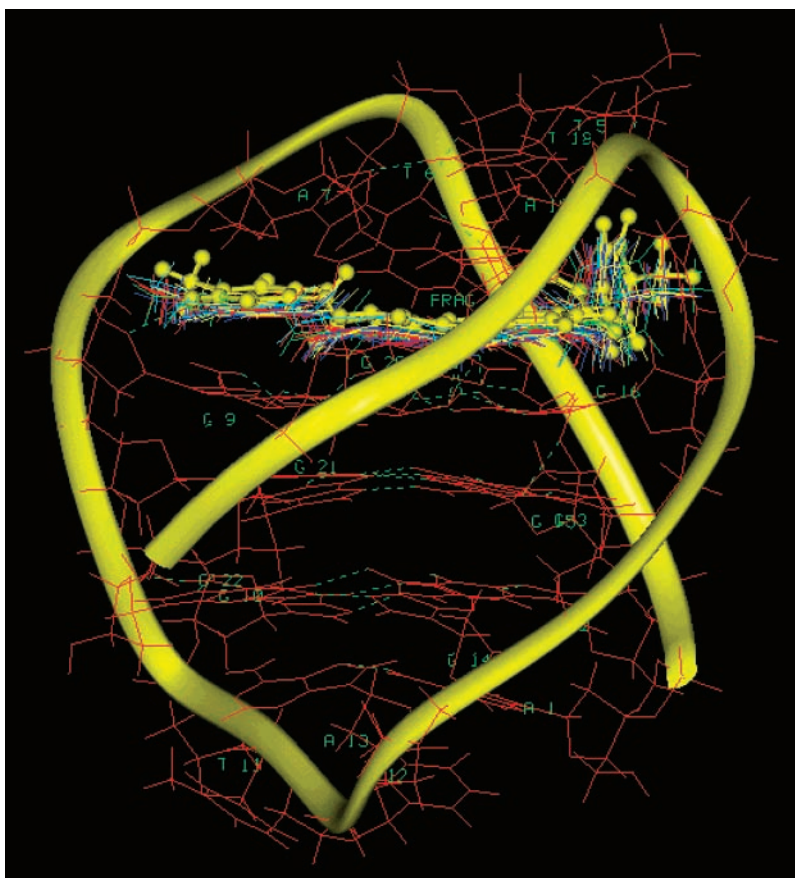
Figure 8. Plot of the superposition of the orientations of BMVC taken from snapshots during the molecular dynamics simulation at 300 K.

TABLE 3: Relative Binding Energies (kcal/mol) for BMVC[a]

position	BMVC + DNA + ions in water system			BMVC + ions in water system			relative binding energy
	vdW	electrostatic	total	vdW	electrostatic	total	
parallel loop	−132.55	−269.31	−401.86	−73.15	−244.19	−317.34	−84.52
diagonal loop	−121.33	−265.07	−386.40	−73.15	−244.19	−317.34	−69.06
wide groove	−84.99	−255.51	−340.5	−73.15	−244.19	−317.34	−23.16
narrow groove	−87.06	−243.69	−330.75	−73.15	−244.19	−317.34	−13.41
top parallel loop	−80.62	−245.30	−325.92	−73.15	−244.19	−317.34	−7.96
parallel loop + diagonal loop	p: −117.25	−256.17	−373.42	−73.15	−244.19	−317.34	−116.59
	d: −107.24	−270.61	−377.85				

[a] p: parallel loop. d: diagonal loop.

groove, two medium groove, one narrow groove, and top parallel loop binding sites. Our molecular modeling shows that the end-stacked binding sites in the parallel and diagonal loops have the highest affinity and are more favorable; the groove binding sites are significantly less stable than the end-stacked binding sites. To find an intercalated site, we attempted to stack one pyridinium of the BMVC at one end of the quartet and dock the rest of BMVC to quadruplex groove; this was called L shape binding to the wide groove, and has a binding energy of −80.36 kcal/mol. Similarly, the binding energy when the drug is on top of the parallel loop is −57.50 kcal/mol. Furthermore, we were unable to obtain a reasonable value for intercalation between the two quartet planes, because the space is small and not allowable using the program. For convenience, the minimized complex structures for these various binding sites are presented in Figure 3, and these are (a) the narrow groove, (b) the wide groove, (c) the top parallel loop, and (d) the L shape wide groove. In this figure, surface electrostatic potential of each structure at pH 7.0 is also displayed. As can be seen directly

from Figure 3, the carbazole part and pyridinium rings of BMVC are oriented on the groove and exhibit steric interactions with the phosphate backbone.

Our initial SA docking modeling studies show that the interaction of both the BMVC and G quadruplex undergoes conformational adjustment that led to significant changes in their relative position, orientation, and binding energy. Using a 1:1 stoichiometry of the BMVC−G-quadruplex complex in the parallel loop that is shown in Figure 4, it appears that the central carbazole moiety of BMVC can well form a sandwich-like stack with the G20 base of the G quartet and the A19 base of the TTA loop and, furthermore, one of the pyridinium arms of BMVC stacks with the G8 base of the G quartet, and the second pyridinium reorients perpendicularly in order to stack on the T17 base in the TTA loop. BMVC-induced rearrangements corresponding to local changes in G-quadruplex structure can also be observed in the diagonal loop, and this is shown in Figure 5. Here, the carbazole moiety of BMVC can well form a sandwich-like stack with the G14 and G22 bases of the G
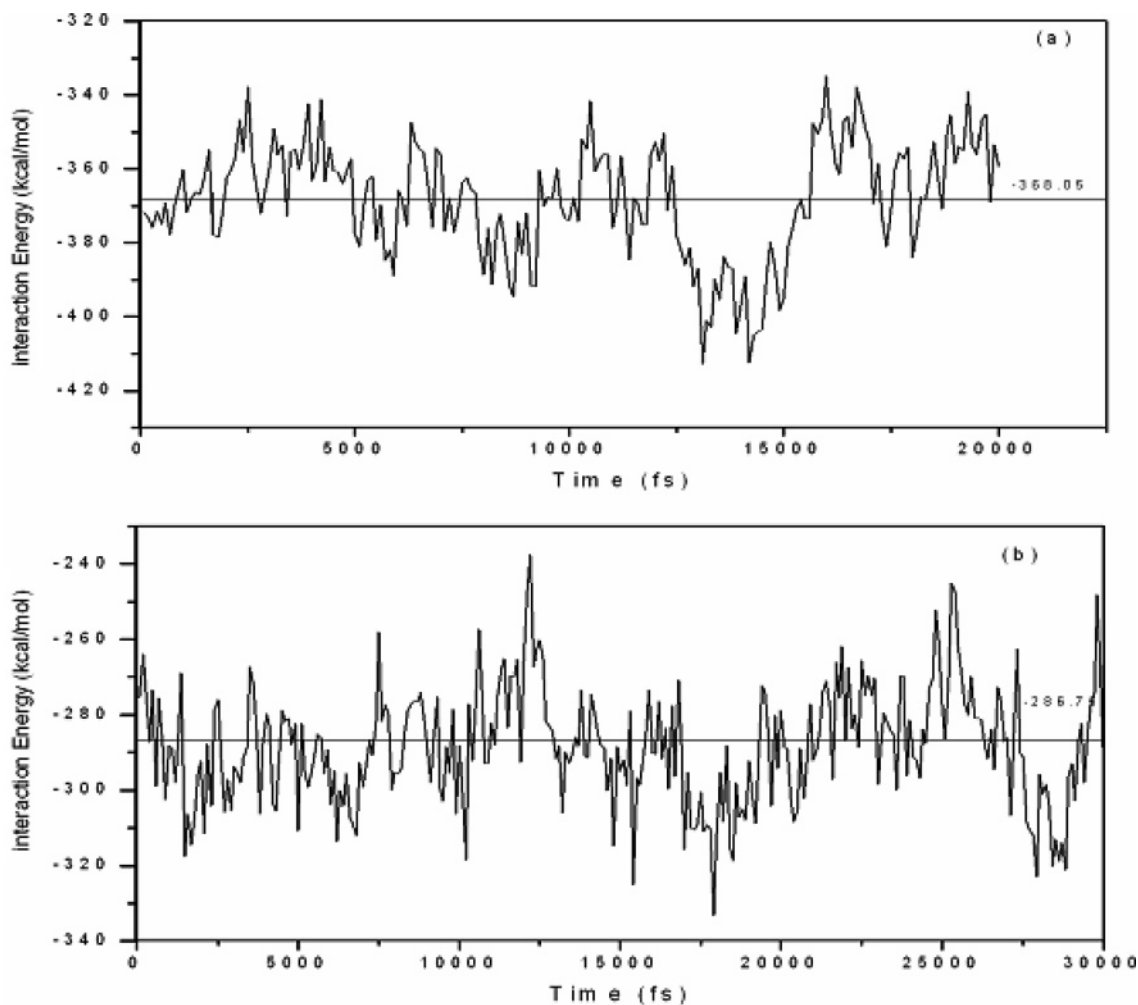
Figure 9. Plot of the fluctuation of the binding energy for the BMVC−G-quartet complex in the parallel loop.

quartet and the A13 base of the TTA loop together with one pyridinium ring of BMVC stacking with the G10 base of the G quartet, but with no stacking found for the second pyridinium ring. Interestingly enough, we also found that the pyridinium ring, when attached to the BMVC, shows strongly favorable steric interaction with the base of the loop. The stacked distances are listed in Table 2, and the values are quite close to those found for DNA bases at about 3.63 Å. From the binding energy point of view, the binding site in the parallel loop is a little stronger than that in the diagonal loop.

Figures 6a and 6b show the conformational comparison of the BMVC bound and free structures of the G quadruplex in the parallel loop and in the diagonal loop, individually. In this respect, the root-mean-square deviations of the conformational comparison in the parallel loop and in the diagonal loop are 1.5225 and 1.5233 Å, respectively. The green ribbon shows the free bound structure. BMVC-induced local loop changes corresponding to a pulling out of the loop and an increasing of the space in G-quadruplex structure are observed.

Moreover, a 2:1 model of two BMVCs bound with one G quadruplex in the end-stacked model is shown in Figure 7. The presence of the BMVC molecule in the diagonal loop favored a change in the parallel loop, because of the presence of the 5′ and 3′ ends of sequence in the diagonal loop. Once the BMVC enters the parallel loop site, the stacking interaction is stronger than in the diagonal loop. It is important to compare how easily the BMVC is able to enter into the parallel or diagonal loop sites, and we will discuss this kinetic problem in our future work.

Our analysis reveals that the presence of a second BMVC molecule further increases the overall binding energy of the 1:1 complex from −128.17 to −244.82 kcal/mol for the 2:1 complex.

We found that the BMVC compound investigated in this work is of special interest. Basically, the SA docking and subsequent molecular dynamics simulation studies show an intriguing binding model where the planar aromatic substituents of BMVC are stabilized by π−π stacking interactions with the G quartet. This supports the hypothesis that these directly stack on the G quartet planes and TTA bases on loops, and this may be involved in increasing the interaction energy. Particularly, BMVC is able to bind effectively due to the two pyridinium rings at the ends of the two side chains, which are able to enhance the π−π stacking interactions. This suggests that the optimal chain length is about 4−5 carbon atoms and it can easily rotate to maximize any nonbonding interactions. All of these findings agree well with the experimental results, which show that BMVC interacts and thermally stabilizes the folded G-quadruplex structure. Other longer chains and different derivatives will be discussed in our future work. Generally speaking, our model suggests that any substituent at this position will potentially introduce steric hindrances with the adjacent G quartet and interfere with the essential 3.6 Å stacking interactions. Moreover, the π−π stacking interaction conjugates with the ring system and maintains planarity at the edge of the G quartet. Therefore, BMVC is a good stabilizer for the folded G-quadruplex structure and is a potent telomerase inhibitor.

Human Telomere and Carbazole Derivative Interaction

J. Phys. Chem. A, Vol. 111, No. 38, 2007 **9231**

TABLE 4: Comparison of the Relative Binding Energies (kcal/mol) in the Parallel Loop

compound	drug + DNA + ions water system			drug + ions water system			relative binding energy
	vdW	electrostatic	total	vdW	electrostatic	total	
BMVC[a]	−132.55	−269.31	−401.86	−73.15	−244.19	−317.34	−84.52
PBMVC[b]	−117.56	−5.92	−123.48	−54.19	−9.62	−63.81	−59.67
AC[c]	−124.19	−421.27	−545.46	−56.42	−431.98	−488.4	−57.07[d]

[a] BMVC: 3,6-bis(1-methyl-4-vinylpyridinium iodine carbazole). [b] PBMVC: BMVC precursor. [c] AC: acridine chromophore. [d] Neidle et al.[16] obtained an estimated value of −68.6 kcal/mol for AC.

Based on the average of dynamics trajectory analysis, the relative binding energies for BMVC interacting with the G quadruplex at the different binding sites in an aqueous system are listed in Table 3. For these binding sites, there is an increasing trend in relative binding energy as the binding sites move from the surface to the end-stacked sites. It appears that the major binding sites involve either the parallel or diagonal loops or both, because there are higher relative binding energies at those binding sites. In Figure 8, we plot the superposition of the orientations of BMVC, taken from snapshots during the dynamics simulation at 300 K. Fluctuations in the binding energy for the BMVC−G-quartet complex in the parallel loop are extracted for Figure 9. In Table 4, we compared the relative binding affinities for BMVC, the BMVC precursor (PBMVC) (Figure 1b), and the acridine chromophore (AC) (Figure 1c)[16] in the parallel loop site. This is done while the drug was bound to the folded hum22 telomeric DNA G-quadruplex structure and is calculated by subtracting the total averaged interaction energy of the explicitly solvated drug and ions in a water periodic box using an identical system for each drug. During our simulation, the structure of BMVC precursor is known to have no methyl group on the pyridinium chain, and hence it is neutral. Neidle et al. (1999) obtained a relative binding energy for AC of −68.6 kcal/mol.[16] According to our calculation, the relative binding energy of AC is −57.07 kcal/mol. Specifically, for BMVC and PBMVC, the relative binding energies are −84.52 and −59.67 kcal/mol in parallel loop structure, respectively. Thus, it is apparent that the pyridinium rings of BMVC dominate the contribution of the binding interaction between drug and DNA. Moreover, the $\pi-\pi$ stacking interaction through electronic interaction stabilizes the planarity of the G quartet. This confirms our argument that the charge effect is important, too.

IV. Conclusion

In summary, BMVC is a potent designed compound that is intended to be used as a telomerase inhibitor and would seem to act by stabilizing G-quadruplex structures. The G-quadruplex interactions of BMVC are more stable in terms of the intramolecular structure in contrast to other G-quadruplex interactive compounds.[15] Our molecular dynamics simulations show that the drug is firmly bound within site, and that key stacking and hydrogen-bonding interactions are maintained. One should be aware of the fact that the charge effect is important. Here the $\pi-\pi$ stacking interaction stabilizes the ring system and BMVC is sandwiched between the loop and the quartet plane so that planarity relative to the edge of the G quartet is maintained. Furthermore, our analysis of the dynamic trajectories reveals that the binding of a second drug molecule is able to further increase overall binding affinity.

References and Notes

(1) (a) Blackburn, E. H. *Nature* **1991**, *350*, 569−573. (b) Blackburn, E. H.; Greider, C. W. *Telomeres*; Cold Spring Harbor Laboratory Press: New York, 1996. (c) Blackburn, E. H.; Szostake, J. W. *Annu. Rev. Biochem.* **1984**, *53*, 163−194. (d) Williamson, J. R. *Annu. Rev. Biophys. Biomol. Struct.* **1994**, *23*, 703−730. (e) McEachern, M. J.; Krauskopf, A.; Blackburn, E. H. *Annu. Rev. Genet.* **2000**, *34*, 331−358.

(2) (a) Harley, C. B.; Futcher, A. B.; Greider, C. W. *Nature* **1990**, *345*, 458−460. (b) Allsopp, R. C.; Harley, C. B. *Exp. Cell Res.* **1995**, *219*, 130−136.

(3) (a) Lundblad, V.; Szostak, J. W. *Cell* **1989**, *57*, 633−643. (b) Sandell, L. L.; Zakian, V. A., *Cell* **1993**, *75*, 729−739. (c) Harley, C. B.; Villeponteau, M. P. *Curr. Opin. Genet. Dev.* **1995**, *5*, 249−255.

(4) (a) O'Reilly, M., Teichmann, S. A.; and Rhodes, D. *Curr. Opin. Struct. Biol.* **1999**, *9*, 58−65. (b) Greider, C. W.; Blackburn, E. H. *Cell* **1987**, *51*, 887−898. (c) Feng, J.; Funk, W. D.; Wang, S.-S.; Weinrich, S. L.; Avilion, A. A.; Chiu, C.-P.; Adams, R. R.; Chang, E.; Allsopp, R. C.; Yu, J.; Le, S.; West, M. D.; Harley, C. B.; Andrews, W. H.; Greider, C. W.; Villeponteau, B. *Science* **1995**, *269*, 1236−1241.

(5) (a) Kim, N. W.; Piatyszek, M. A.; Prowse, K. R.; Harley, C. B.; West, M. D.; Ho, P. L. C.; Coviello, G. M.; Wright, W. E.; Weinrich, R.; and Shay, J. W. *Science* **1994**, *266*, 2011−2015. (b) Meyerson, M.; Counter, C. M.; Eaton, E. N.; Ellison, L. W.; Steiner, P.; Caddle, S. D.; Ziaugra, L.; Beijersbergen, R. L.; Davidoff, M. J.; Lie, Q.; Bacchetti, S.; Haber, D. A.; and Weinberg, R. A. *Cell* **1997**, *90*, 785−795.

(6) (a) Hahn, W. C.; Stewart, S. A.; Brooks, M. W.; York, S. G.; Eaton, E. Kurachi, A. Beijersbergen, R. L.; Knoll, J. H. M.; Meyerson, M.; and Weinberg, R. A. *Nat. Med.* **1999**, *5*, 1164−1170. (b) Zhang, X.; Mar, V.; Zhou, W.; Harrington, L.; and Robinson, M. O. *Genes Dev.* **1999**, *13*, 2388−2399.

(7) Herbert, B. S.; Pitts, A. E.; Baker, S. I.; Hamilton, S. E.; Wright, W. E.; Shay, J.; Corey, D. R. *Proc. Natl. Acad. Sci. U.S.A.* **1999**, *96*, 14276−14281.

(8) Neidle, S.; Kelland, L. R. *Anti-Cancer Drug Des.* **1999**, *14*, 341−347.

(9) (a) Mergny, J. L.; Hélène, C. *Nat. Med.* **1998**, *4*, 1366−1367. (b) Han, H. Y.; Hurley, L. H. *Trends Pharmacol. Sci.* **2000**, *21*, 136−142.

(10) Meyne, J.; Ratliff, R. L.; Moyzis, R. K. *Proc. Natl. Acad. Sci. U.S.A.* **1989**, *86*, 7049−7053.

(11) Morin, G. B. *Cell* **1989**, *59*, 521−529.

(12) Gellert, M.; Lipsett, M. N.; Davies, D. R. *Proc. Natl. Acad. Sci. U.S.A.* **1962**, *48*, 2013−2018.

(13) Zahler, A. M.; Williamson, J., R.; Cech, T. R.; Prescott, D. M. *Nature* **1991**, *350*, 718−720.

(14) (a) Fletcher, T. M.; Sun, D.; Salazar, M.; Hurley, L. H. *Biochemistry* **1998**, 37, 5536−5541. (b) Sun, D.; Lopez-Guajardo, C. C.; Quada, J.; Hurley, L. H.; Von Hoff, D. D. *Biochemistry* **1999**, *38*, 4037−4044.

(15) (a) Sun, D.; Thomp son, B.; Cathers, B. E.; Salazar, M.; Kerwin, S. M.; Trent, J. O.; Neidle, S.; Hurley, L. H. *J. Med. Chem.* **1997**, *40*, 2113−2116. (b) Perry, P. J.; Gowan, S. M.; Reszka, A. P.; Polucci, P.; Jenkins, T. C.; Kelland, L. R.; Neidle, S. *J. Med. Chem.* **1998**, *41*, 3253−3260. (c) Zewail-Foote, M.; Hurley, L. H. *J. Am. Chem. Soc.* **2001**, *123*, 6485−6495. (d) Shi, D.-F.; Wheelhouse, R. T.; Sun, D.; Hurley, L. H. *J. Med. Chem.* **2001**, *44*, 4509−4523. (e) Koeppel, F.; Riou, J.-F.; Laoui, A.; Mailliet, P.; Arimondo, P. B.; Labit, D.; Petitgenet, O.; Hélène, C.; Mergny, J.-L. *Nucleic Acids Res.* **2001**, *29*, 1087−1096. (f) Read, M.; Harrison, J. R.; Romabnoli, B.; Tanious, F. A.; Gowan, S. H.; Reszka, A. P.; Wilson, W. D.; Kelland, L. R.; Neidle, S. *Proc. Natl. Acad. Sci. U.S.A.* **2001**, *98*, 4844−4849.

(16) Read, M.; Wood, A. A.; Harrison, J. R.; Gowan, S. H.; Kelland, L. R.; Dosanjh, H. S.; Neidle, S. *J. Med. Chem.* **1999**, *42*, 4538−4546.

9232 *J. Phys. Chem. A, Vol. 111, No. 38, 2007*

Yang et al.

(17) Mergny, J. L.; Lacroix, L.; Teulade-Fichou, M.-P.; Hounsou, C.; Guittat, L.; Hoarau, M.; Arimondo, P. B.; Vigneron, J.-P.; Lehn, J.-M.; Riou, J.-F.; Garestier, T.; Hélène, C. *Proc. Natl. Acad. Sci. U.S.A.* **2001**, *98*, 3062−3067.

(18) Chang, C. C.; Wu, J. Y.; Chang, T.-C. *J. Chin. Chem. Soc.* **2003**, *50*, 185−188.

(19) Chang, C. C.; Wu, J. Y.; Chien, C. W.; Wu, W. S.; Liu, H.; Kang, C. C.; Yu, L. J.; Chang, T.-C. *Anal. Chem.* **2003**, *75*, 6177−6183.

(20) Chang, C. C.; Kuo, I.-C.; Ling, I.-F.; Chen, C. T.; Chen, H. C.; Lou, P. J.; Lin, J. J.; Chang, T.-C. *Anal. Chem.* **2004**, *76*, 4490−4494.

(21) Chang, C. C.; Chu, J. F.; Kao, F. J.; Chiu, Y. C.; Lou, P. J.; Chen, H. C.; Chang, T.-C. *Anal. Chem.* **2006**, *78*, 2810−2815.

(22) (a) Kang, C.-C.; Chang, C.-C.; Cheng, J.-Y.; Chang, T.-C. *J. Chin. Chem. Soc.* **2005**, *52*, 1069−1072. (b) Chang, C. C.; Chu, J. F.; Kuo, H. H.; Kang, C.-C.; Lin, S. H.; Chang, T. C. *J. Lumin.* **2006**, *119−120*, 84−90.

(23) Chang, C. C.; Kuo, I-C.; Lin, J.-J.; Lu, Y.-C.; Chen, C.-T.; Back, H.-T.; Lou, P.-J.; Chang, T.-C. *Chem. Biodiversity* **2004**, *1*, 1377−1384.

(24) Wheelhouse, R. T.; Sun, D.; Han, H.; Han, F. X.; Hurley, L. H. *J. Am. Chem. Soc.* **1998**, 120, 3261−3262.

(25) Riou, J.-F.; Guittat, L.; Mailliet, P.; Laoui, A.; Renou, E.; Petitgenet, O.; Mègnin-Chanet, F.; Hélène, C.; Mergny, J. L. *Proc. Natl. Acad. Sci. U.S.A.* **2002**, *99*, 2672−2677.

(26) Kim, M. Y.; Vankayalapati, H.; Shin-Ya, K.; Wierzba, K.; Hurley, L. H. *J. Am. Chem. Soc.* **2002**, 124, 2098−2099.

(27) Gavathiotis, E.; Heald, R. A.; Stevens, M. F. G.; Searle, M. S. *Angew. Chem., Int. Ed.* **2001**, 40, 4749−4751.

(28) (a) *INSIGHTII Modelling Environment*; Molecular Simulations Inc. (MSI): 1984. (b) Dauber-Osguthorpe, P.; Roberts, V. A.; Osguthorpe, D. J.; Wolff, J.; Genest, M.; Hagler, A. T. *Proteins: Struct., Funct., Genet.* **1988**, *4*, 31−47.

(29) Wang, Y.; Patel, D. J. *Structure* **1993**, 1, 263−282.

(30) Jorgensen, W. L.; Chandrasekhar, J.; Madura, J. D.; Impey, R. W.; Klein, M. L. *J. Chem. Phys.* **1983**, 79, 926−935.

(31) (a) Ding, H.-Q.; Karasawa, N.; Goddard, W. A. *J. Chem. Phys.* **1992**, 97, 4309−4315. (b) Esselink, K. *Inf. Process. Lett.* **1992**, 41, 141−147. (c) Greengard, L.; Rokhlin, V. *J. Comput. Phys.* **1987**, *73*, 325−348.

(32) Ryckaert, J. P.; Ciccotti, G.; Berendsen, H. J. C. *J. Comput. Phys.* **1977**, 23, 327−341.